Biotechnology Reports 3 (2014) 60–64

Contents lists available at ScienceDirect

Biotechnology Reports

journal homepage: www.elsevier.com/locate/btre

Recrystallization inhibition in ice due to ice binding protein activity detected by nuclear magnetic resonance

Jennifer R. Brown [a,e,*], Joseph D. Seymour [a,e], Timothy I. Brox [a], Mark L. Skidmore [b], Chen Wang [c], Brent C. Christner [c], Bing-Hao Luo [c], Sarah L. Codd [d,e]

[a] Chemical and Biological Engineering Department, Montana State University, Bozeman, MT 59717, USA
[b] Earth Sciences Department, Montana State University, Bozeman, MT 59717, USA
[c] Department of Biological Sciences, Louisiana State University, Baton Rouge, LA 70803, USA
[d] Mechanical and Industrial Engineering Department, Montana State University, Bozeman, MT 59717, USA
[e] Center for Biofilm Engineering, Montana State University, Bozeman, MT 59717, USA

ARTICLE INFO

Article history:
Received 14 March 2014
Received in revised form 11 June 2014
Accepted 12 June 2014
Available online 20 June 2014

Keywords:
Nuclear magnetic resonance
Ice
Ice binding protein
Cryopreservation
Recrystallization

ABSTRACT

Liquid water present in polycrystalline ice at the interstices between ice crystals results in a network of liquid-filled veins and nodes within a solid ice matrix, making ice a low porosity porous media. Here we used nuclear magnetic resonance (NMR) relaxation and time dependent self-diffusion measurements developed for porous media applications to monitor three dimensional changes to the vein network in ices with and without a bacterial ice binding protein (IBP). Shorter effective diffusion distances were detected as a function of increased irreversible ice binding activity, indicating inhibition of ice recrystallization and persistent small crystal structure. The modification of ice structure by the IBP demonstrates a potential mechanism for the microorganism to enhance survivability in ice. These results highlight the potential of NMR techniques in evaluation of the impact of IBPs on vein network structure and recrystallization processes; information useful for continued development of ice-interacting proteins for biotechnology applications.

1. Introduction

Proteins with ice-interacting activity have been identified in fish, cold hardy plants and insects [1–3], and certain cold-adapted bacteria, diatoms, and algae [4]. The properties of ice-interacting proteins are useful in many areas of biotechnology, including cell line cryopreservation [5] and food manufacturing [6]. Understanding their affect on ice and recrystallization processes is critical for further development in both applied and basic applications. The cold tolerant bacterium 3519-10 (Flavobacteriaceae family), isolated from basal ice recovered from the Vostok 5G ice core [7], secretes an extracellular ice binding protein (IBP) that binds to the ice crystal prism face and inhibits growth along the *a*-axis [8]. The 3519-10 IBP has been shown to increase bacterial viability during freeze and thaw cycling [9]; however, its mechanism of action and impact on the internal pore structure of unfrozen water in ice is not well understood.

Within polycrystalline ice, liquid unfrozen water is located at interfaces between two or three hexagonal ice crystals due to the presence of impurities [10,11]. At triple grain junctions, veins form that may be approximated as cylinders with diameters, d_{vein} which can be related to ice crystal diameters d via liquid water fraction $f = 6\pi\sqrt{2}((1/2d_{vein})/d)^2$ [12]. Where two grains meet, a planar junction of thickness d_{plane} forms on the octahedra faces. As ice ages, it undergoes a thermodynamically driven coarsening, termed recrystallization, whereby larger ice crystals grow at the expense of smaller ones, altering vein dimensions [13,14]. Ice is therefore a complex and dynamic low porosity porous media, where ice crystals compose the solid matrix and liquid veins the pore space. With non-invasive and non-destructive nuclear magnetic resonance (NMR) techniques, the vein network can be directly characterized. With respect to biotechnology applications, Kirsebom *et al.* have shown the utility of NMR to monitor the composition of the unfrozen water phase during the formation of cryogels *in situ* [15,16]. We utilize NMR magnetic relaxation time and molecular diffusion measurements, which are proven robust in probing pore structure in porous media [17] and sensitive to vein

* Corresponding author at: Montana State University, Chemical and Biological Engineering, 306 Cobleigh Hall, PO Box 173920, Bozeman, MT 597173920, USA. Tel.: +1 406 994 7719.
E-mail address: jbrown@coe.montana.edu (J.R. Brown).

http://dx.doi.org/10.1016/j.btre.2014.06.005

dimensions [18], to provide a novel method for monitoring ice structure and its evolution with time. This provides a new analytical method for quantitative characterization of ice structure during biotechnological freezing processes.

Here we have applied advanced NMR techniques to ice samples, establishing them as methods to physically characterize ice vein network structure. These techniques were then used to examine the impact of IBP on bulk liquid vein network structure in order to improve our understanding of the impact of this ice-interacting protein on recrystallization processes. Our findings have implications for geophysical modelling of frozen systems [4] and in development of IBPs for biotechnology applications [6]. Also, with advances in design of portable NMR systems including Earth's field systems [19], low field permanent magnets [20] and surface NMR [21], our research highlights the potential for using these methods in biotechnology process monitoring.

2. Materials and methods

2.1. Extracellular protein (ECP) and rIBP preparation

Extra cellular proteins (ECP) and the recombinant IBP (rIBP) from isolate V3519 for use in the ice experiments were prepared as follows. For ECP, the V3519-10 bacteria were grown in R2 liquid media at 4 °C until the culture reached an optical density OD_{595} of 0.22 at which time it was centrifuged at 5000 g for 30 min at 4 °C to pellet the cells and recover the supernatant. The supernatant containing the IBP was filtered using Amicon Ultra-15 centrifugal filters with a nominal threshold of 30 kDa to obtain a crude extract of V3519-10's extracellular proteins. Protein concentrations were determined with the Bradford assay using the Coomassie Plus reagent. For the rIBP, the cDNA encoding IBP without the signal peptide but with a 6× His tag added to the C-terminus was cloned into the pET-21a expression vector (Novagen) and transformed into BL21 cells. The BL 21 cells were cultured in LB medium at 37 °C to an optical density of 0.8, when isopropyl β-D-1-thiogalactopyranoside was added to give a final concentration of 1 mM and the temperature was reduced to 18 °C. Proteins were extracted from the cell culture after incubating overnight and the rIBP was purified as described previously [22]. The purified protein size (~52 kDa) was determined via sodium dodecyl sulfate polyacrylamide gel electrophoresis (SDS-PAGE) and its concentration was measured using spectrophotometry (NanoDrop ND-1000).

2.2. Ice sample preparation

Five ice samples were prepared. All samples contained a 7 g/l NaCl solution, which is a salt concentration comparable with measurements in Antarctic basal ice [23]. IBPs were added to three samples to monitor concentration effects and the difference between naturally secreted extracellular protein (ECP) and purified recombinant IBP (rIBP). The ice sample containing a crude preparation of the IBP consisted of 7 g/l NaCl solution with 10 μg/ml of 3519-10 ECP (>30 kDa with an unknown IBP fraction) and will hereafter be referred to as ice with ECP. The two samples containing 7 g/l NaCl and 2 and 4 μg/ml recombinant IBP will be referred to as ice with rIBP(2) and ice with rIBP(4) respectively. Two control samples were also prepared: (i) the ice control, a 7 g/l NaCl solution without protein and (ii) ice with bovine serum albumin (BSA), a 7 g/l NaCl solution with 10 μg/ml BSA. The second control was used to examine ice binding activity from colligative effects due to the presence of a similar macromolecule, since BSA is of similar size (~64 kDa) to the 3519-10 IBP (~52 kDa), but does not exhibit ice binding activity. All samples were prepared by filling 13 mm OD (11.7 mm ID) standard NMR tubes with solution, placing them in a polystyrene sample holder, insulated on the sides and bottom, and freezing them in a Revco ULT-750 chest freezer at −13.5 °C. To ensure hexagonal ice crystal structure consistent between sample types, multiple samples of each concentration were frozen and inspected by eye and those with cloudiness and/or air bubbles which would indicate supercooling and subsequent rapid freezing were discarded. Samples were transferred from the chest freezer in a cooler filled with gel freezer packs stored in the same freezer. Transfer time of the ice from the cooler to being in the RF coil with cold nitrogen gas flow was minimized to ~3 min. The MR magnet electronics were always pre-cooled at the set temperature before sample insertion and the set temperature equilibrized within ~5 min. The samples were allowed to equilibrate at the set temperature for 45 min before measurements were performed. Samples were analysed via NMR at multiple time points over 1800 h, and stored in the freezer at −13.5 °C in between NMR measurements.

2.3. NMR methods

NMR measurements were performed on a Bruker DRX250 spectrometer with a 5.8 T superconducting vertical wide bore magnet and Micro2.5 gradient imaging probe capable of producing maximum gradients of $1\,T\,m^{-1}$. Temperature was controlled via flow of cooled nitrogen gas along the vertical axis of the NMR sample tube using a Bruker variable temperature control unit. The 13 mm OD (11.7 mm ID) frozen ice samples were centred in a 20 mm diameter radiofrequency coil using polyether ether ketone (PEEK) spacers to allow for constant and consistent air flow around the sample. The set point temperature was −15 °C at the base of the coil and the temperature increase of the cooled nitrogen gas was ~7° C across the full coil length. Unfrozen water content was calculated from the NMR signal magnitude after calibration with a known volume of water at the same receiver gain as a function of temperature. Signal from the solid ice crystals was not detectable. The FID decay was single exponential, i.e. from liquid water only, no solid state Gaussian signal from the ice phase was detected due to the rf excitation and signal acquisition digitization time scales. Cross-relaxation between the solid ice crystal phase and liquid water in veins can be neglected based on this and the large difference between the water diffusivity $\sim 10^{-10}\,m^2\,s^{-1}$ and the spin diffusion $\sim 10^{-15}\,m^2\,s^{-1}$ [24]. T_2 relaxation time distributions were obtained using a standard Carr–Purcell–Meiboom–Gill (CPMG) echo train with echo time $t_E = 403$ μs. A standard pulsed gradient stimulated echo (PGSTE) sequence was used to measure diffusion for displacement observation times Δ ranging from 10–1000 ms at a constant echo time t_E of 8 ms and gradient duration $\delta = 2$ ms. Gradients were applied in the horizontal y-direction, perpendicular to the tube walls, in order to eliminate the impact of any anisotropy on the measurements from crystal elongation in the z-direction due to the top-down freezing process. Diffusion coefficients were calculated from a standard Stejskal–Tanner plot and the fit was linear with no indication of multiexponential decay. The mono-exponential decay was also confirmed by performing an inverse Laplace transform which resulted in a single diffusion coefficient. Images were obtained with a standard 2D multi-slice spin echo sequence and had a spatial resolution of 55 × 55 μm (256 × 256 matrix size and 14 × 14 mm field of view) over a 0.5 mm slice centred in the middle of the rf coil.

3. Results

Fig. 1, top row, shows cross-sectional magnetic resonance images acquired for ice with BSA at various time intervals after freezing. Definitive ice crystal growth during recrystallization was observed over 1800 h, with crystal diameters growing from

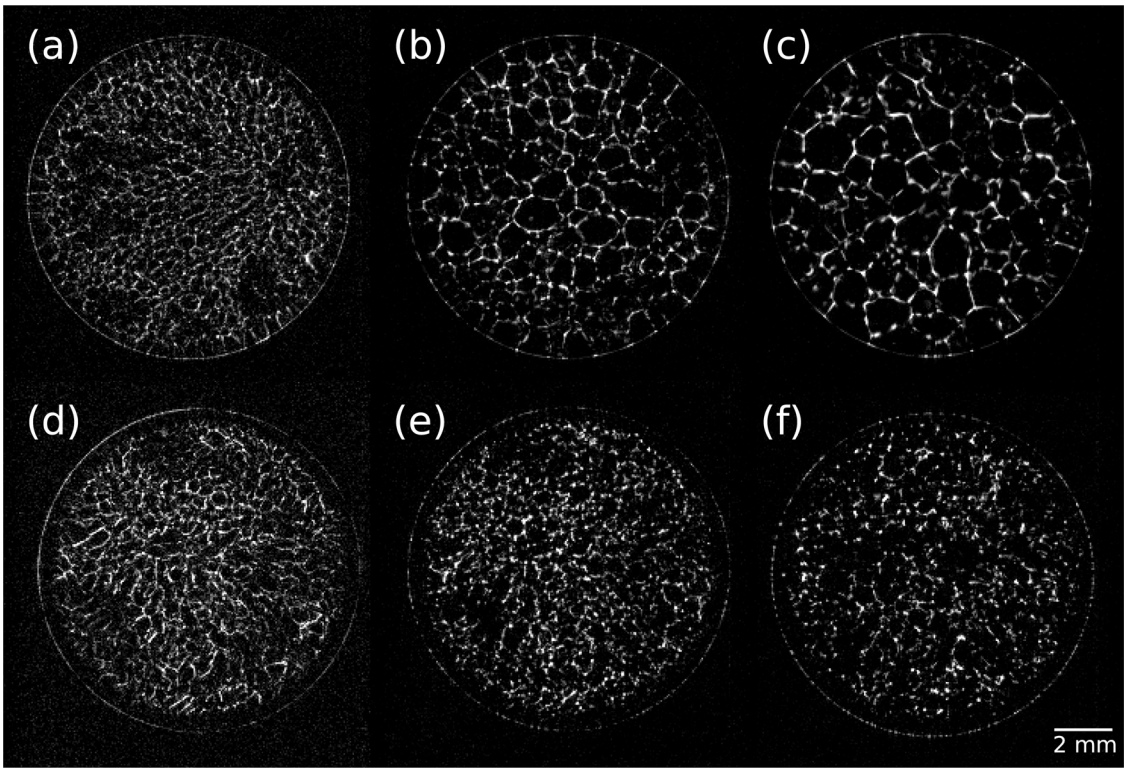

Fig. 1. Cross-sectional MR images of vein networks in ice samples at −13.5 °C for aging to 1730 h after initial freezing. Spatial resolution is 55 × 55 μm over a 14 × 14 mm FOV and 0.5 mm slice. Top: Ice with BSA (10 μg/ml). Left to right (a)–(c): t = 39, 578 and 1705 h. Ice crystal growth from ∼200 μm to 1 mm clearly occurs over this time period. Bottom: Ice with ECP (∼10 μg/ml extracellular protein extract containing an unknown fraction of IBP). Left to right (d)–(f): t = 102, 651 and 1730 h. Inhibition of ice crystal growth is clear over this time period.

∼200 μm to ∼1 mm. The ice control showed identical behaviour. In contrast, ice with ECP, bottom row, exhibited static crystal structure, ostensibly due to IBP binding to the ice crystal surface inhibiting crystal growth [8].

In the ice with rIBP(2) and rIBP(4), ice crystals were smaller, an indication of increased activity of purified IBP over ECP. Vein diameters in the ice with rIBP samples were below the 55 μm spatial resolution of the Fig. 1 images, the lowest practically achievable with MRI on these samples due to signal to noise and experiment time limitations [25]. These data clearly demonstrate that the 3519-10 IBP alters the ice crystal structure and therefore the unfrozen vein network, or interstitial habitat for microbial cells, in ice.

NMR measurements of spin–spin magnetic relaxation time (T_2) and molecular diffusion are alternatives to MRI visualization and provide quantitative information about the vein network structure. T_2 times are measured from signal arising from the entire volume of the ice sample and therefore represent an average over the three dimensional pore space. They also have the advantage of rapid acquisition. A liquid phase confined within a solid matrix exhibits spin–spin relaxation times shortened in a manner dependent on pore size [17,25]. T_2 amplitude is proportional to a pore length scale l_p, scaling as $1/T_2 \sim \rho S/V_p \sim 1/l_p$ [26], where S is pore surface area, V_p pore volume and the constant of proportionality ρ is the surface relaxivity. This proportionality theoretically only holds in the regime where diffusional mixing of the surface and bulk fractions is faster than the difference in intrinsic relaxation rates. With a liquid phase diffusion of 5.6×10^{-10} m^2 s^{-1}, the diffusional mixing is on the order of 10–100 ms which is indeed faster than the relaxation rate difference. For ice, the rate of change of T_2 is related to recrystallization kinetics. Therefore, relative changes in T_2 relaxation during ice aging indicate changes in vein dimensions due to microstructural rearrangement during recrystallization.

Purified rIBP clearly inhibited growth in the liquid vein size. T_2 values, and therefore the pore lengthscale l_p, were shortened by a factor of 10 and remained unchanged over time (Fig. 2). T_2 values for the ice control lacking protein and ice with BSA exhibit similar magnitudes and rates of change, indicating that BSA did not inhibit liquid vein growth. Ice with ECP exhibited an increase in T_2 at early times (<200 h) and a plateau to smaller T_2 values than the ice control. This suggests that recrystallization occurs in the ice with ECP until coarsening reduces overall crystal numbers to the point

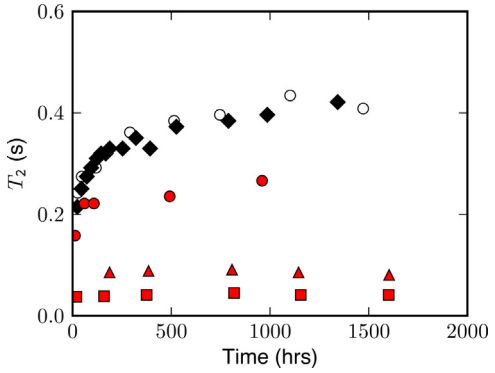

Fig. 2. Evolution of T_2 relaxation times with aging for five ice samples: ice control (filled diamonds), ice with BSA (open circles), ice with ECP (filled circles), ice with rIBP(2) (filled triangles) and ice with rIBP(4) (filled squares). Larger T_2 magnetic relaxation values in the ice control and ice with BSA indicate a larger pore length scale, while shorter T_2 values in the ice with IBP samples and lack of change in relaxation with aging is evidence that IBP inhibits growth of liquid vein size.

where targets on the ice crystal prism face are saturated by IBP. This is consistent with a lower IBP concentration in the ice with crude preparation containing ECP relative to the ice with the purified rIBP.

The geometry of porous media can be probed via measurement with pulsed gradient spin echo (PGSE) NMR [25] of an effective time dependent diffusion coefficient $D\,(\Delta)$ of the restricted liquid [27]. Variation of $D\,(\Delta)$ with changes in displacement observation time Δ reveal pore space structural characteristics [27,28]. In the short displacement time, $\Delta < l_p^2/D_o$, the time dependent diffusion coefficient normalized by molecular diffusion $D\,(\Delta)/D_o$ is proportional to S/V_p due to interaction of liquid molecules in the pore space with boundaries of the solid matrix [28]. Hence, the pore length scale l_p can be estimated as $S/V_p \sim 1/l_p$. Modeling the veins as a cylinder [12], the S/V_p can be calculated as $4/d_{vein}$, resulting in $l_p = d_{vein}/4$. The two grain planar junctions have a S/V_p of $1/d_{plane}$ and therefore a lengthscale $l_p = d_{plane}$. The measured S/V_p represents an average of water confined within the triple and two grain junctions. In the long displacement time, $\Delta \gg l_p^2/D_o$, $D\,(\Delta)/D_o$ asymptotes to $1/\alpha$, where α is geometric tortuosity. Tortuosity is the ratio of the path length a molecule travels in a porous media to the geometric length traversed $\alpha = l_{path}/l_{geom}$ and is a measure of inter-connectivity of the pore space [28]. Here we are limited to observing the approach to asymptotic diffusion, out to $\Delta \sim 1000$ ms due to NMR signal loss via T_1 magnetic relaxation , and therefore measure an effective α.

Fig. 3 shows displacement time dependent diffusion evolution with ice aging for the ice control lacking protein, ice with ECP, ice with rIBP(2) and ice with rIBP(4). The short time slope of the $D\,(\Delta)/D_o$ curve for the ice control yields an effective diffusion distance l_p that increases from 2.5 ± 0.1 μm at $t = 25$ h to 4.2 ± 0.1 μm at 790 h, consistent with ice crystal growth and subsequent larger elongated liquid veins ($l_p = d_{vein}/4$) and planar junction thicknesses ($l_p = d_{plane}$). $D\,(\Delta)/D_o$ of the ice control at $t = 790$ h approaches a larger asymptotic value, or smaller effective tortuosity α. A Padé approximation can be used to interpolate between the short and long time [29,30], resulting in an estimation of tortuosity [29,31]. The Padé fit includes a fitting parameter θ with units of time that represents the time for a particle to diffuse the distance needed to reach the tortuosity limit. For the ice control at $t = 25$ h, α is 4.2, while at $t = 790$ h it decreases to 3.7, consistent with ice crystal coarsening. Ice with BSA (not shown) exhibited similar behaviour to the control sample that lacked protein.

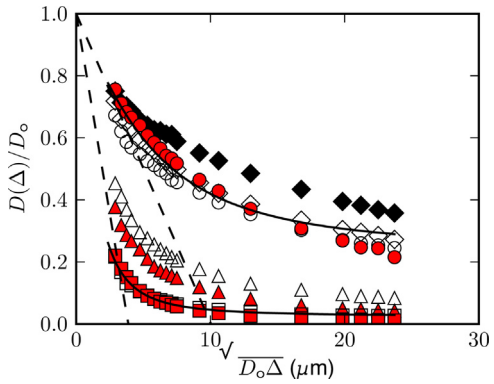

Fig. 3. Displacement time Δ dependent diffusion data with ice aging: ice control (open diamonds, $t = 25$ h; closed diamonds, $t = 1922$ h), ice with ECP (open circles, $t = 92$ h; closed circles, $t = 1909$ h), ice with rIBP(2) (open triangles, $t = 189$ h; closed triangles, $t = 1922$ h) and ice with rIBP(4) (open squares, $t = 20$ h; closed squares, $t = 1914$ h). Dashed lines are the early time fits of S/V_p while solid lines are the Padé approximation fits. Steeper initial slopes indicate larger S/V_p and smaller asymptotic diffusion coefficients imply more restricted motion, consistent with smaller ice crystals and narrower liquid veins.

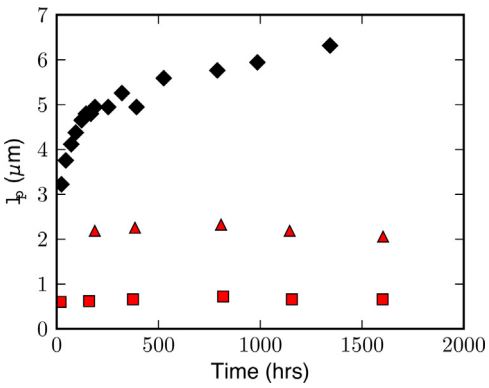

Fig. 4. Pore lengthscale l_p calculated from T_2 relaxation times as a function of ice aging for the ice control (filled diamonds), ice with rIBP(2) (filled triangles) and ice with rIBP(4) (filled squares). Surface relaxivity ρ was found using S/V_p values obtained from the short time fit to the time dependent diffusion data (Fig. 3). A larger pore length scale is observed in the ice control due to ice crystal growth from recrystallization creating larger liquid veins, while shorter lengthscales are evident in the ice with IBP samples where crystal sizes remain small. Lack of change in the lengthscale with aging is evidence that IBP inhibits growth of liquid vein size.

The $D\,(\Delta)/D_o$ behaviour for the ice with rIBP(4) remained stationary over 1000 h. This lack of ice microstructural evolution is evidence of irreversible IBP binding [32], and the longevity of the effect indicates microbial activity is potentially a factor for consideration in ice rheology models where ice structure is a parameter. Ice with rIBP(4) also had the smallest effective diffusion length, $l_p = 1.0 \pm 0.5$ μm, and largest tortuosity, $\alpha = 47.0$, at $t = 819$ h, therefore providing direct experimental evidence of smaller ice crystal structure and smaller liquid veins. Ice with rIBP(2) had $l_p = 1.5 \pm 0.5$ μm and $\alpha = 12.2$ at long times ($t = 810$), while ice with ECP had $l_p = 3.0 \pm 0.5$ μm and $\alpha = 8.9$ at long times ($t = 933$ h). This trend suggests that larger overall crystal sizes and diffusion lengths correlate with decreasing IBP concentration. The $D\,(\Delta)/D_o$ data asymptotes to larger diffusion values (a smaller tortuosity) with decreased IBP concentration, again indicative of larger ice crystals and larger more elongated liquid veins.

Despite microstructural differences due to IBP, water content measured from the liquid state ^{1}H NMR signal [33] was stable between 2 and 2.5% for all samples over 1800 h, in reasonable agreement with the 3% predicted from the equilibrium thermodynamic model FREZCHEM [34]. Bulk water content is therefore an inadequate predictor of ice structure and vein size.

Time dependent diffusion measurements have the advantage of providing quantitative values for physical microstructural parameters (S/V_p and α) relevant to liquid water vein dimensions and corresponding ice crystal sizes. However, experimental acquisition times can be long (~8 h). T_2 relaxation time measurements on the other hand have the advantage of short (~2 min) acquisition times and can provide quantitative values of S/V_p given the surface relaxivity ρ [35]. Surface relaxivity is not an easy parameter to measure. Here, we utilize the quantitative S/V_p obtained from the time dependent diffusion data in Fig. 3 and measured T_2 values to calculate ρ via the relationship $1/T_2 \sim \rho S/V_p$. This is possible, despite the inherent relaxation weighting in PGSE NMR measurements of diffusion that is not present in T_2 relaxation measurements [35], due to the low susceptibility between solid ice and liquid water [18]. Further, the value of ρ was found at both short and long aging times (Fig. 3) and is independent of aging time. As such, the surface relaxivity can be used to calculate S/V_p from T_2 values acquired at aging times where $D\,(t)$ data was not available.

The surface relaxivity for the ice control sample was found to be 1.5×10^{-5} m s^{-1}. Interestingly, ρ for the rIBP(2) and rIBP(4) samples were 2.6×10^{-5} and 1.6×10^{-5} m s^{-1} respectively, indicating that

the IBP attached to the ice crystal surface may change the measured surface relaxivity. Fig. 4 shows $l_p(\sim V_p/S)$ calculated from the T_2 measurements (Fig. 2) as a function of aging for the ice control and rIBP samples. As was inferred from Fig. 2, the ice control lacking protein showed increasing pore lengthscales with aging, consistent with crystal growth and subsequent increases in vein dimensions. With increasing concentrations of IBP, smaller l_p was observed due to the presence smaller crystal sizes, indicating increased inhibition of recrystallization processes.

4. Conclusions

These results demonstrate the ability of non-destructive NMR relaxation and time dependent diffusion measurements to characterize the unfrozen vein network structure and crystal growth processes in ice, as well as its evolution with time. This provides a new quantitative analytical method to assess the impact of biomolecules on ice structure during freezing processes relevant to biotechnological applications. Microbial extracellular IBPs were found to inhibit recrystallization and modify the three dimensional ice structure, resulting in persistent small size ice crystals (observed up to 70 days) and shorter diffusion distances along veins.

These findings have implications to biogeophysical applications examining microbial habitability in ice [9] and also indicate that it is plausible for microbial processes to contribute to persistent small crystal structure in basal ice, which could affect ice rheology [36,37]. Such processes are typically attributed to physicochemical mechanisms [38,39], but microorganisms and their products could have significant but as yet overlooked roles in ice rheology.

Microbial products are increasingly of interest in applications where manipulation of ice crystals is desired, due to their potential for scalability to industrial production [4]. The range of methods, applicable to investigation of ice, make NMR a valuable tool for understanding how ice-interacting proteins impact the three dimensional vein network and recrystallization processes, critical for exploiting the full potential of these proteins in biotechnology applications.

Acknowledgements

JRB and TIB acknowledge the Montana Space Grant Consortium for funding. SLC acknowledges a NSF CAREER award for support. JDS and SLC acknowledge the M.J Murdock Charitable Trust and NSF MRI for instrument funding. BCC was partially supported by grants from NASA (NNX10AN07A and NNX10AR92G) and the NSF (0636828, 0838941, and 1023233). MLS was partially supported by NSF 0636770 and NASA NNX10AT31G.

References

[1] K.V. Ewart, Q. Lin, C.L. Hew, Structure, function and evolution of antifreeze proteins, Cell. Mol. Life Sci. 55 (1999) 271–283.
[2] K.E. Zachariassen, E. Kristiansen, Ice nucleation and antinucleation in nature, Cryobiology 41 (2000) 257–279.
[3] A.K. Brodel, J.A. Raymond, J.G. Duman, F.F. Bier, S. Kubick, Functional evaluation of candidate ice structuring proteins using cell-free expression systems, J. Biotechnol. 163 (2013) 301–310.
[4] B.C. Christner, Bioprospecting for microbial products that affect ice crystal formation and growth, Appl. Microbiol. Biotechnol. 85 (2010) 481–489.
[5] X. Xu, Y. Liu, Z.F. Cui, Y.P. Wei, L. Zhang, Effects of osmotic and cold shock on adherent human mesenchymal stem cells during cryopreservation, J. Biotechnol. 162 (2012) 224–231.
[6] S. Venketesh, C. Dayananda, Properties, potentials, and prospects of antifreeze proteins, Crit. Rev. Biotechnol. 28 (2008) 57–82.
[7] B.C. Christner, E. Mosley-Thompson, L.G. Thompson, J.N. Reeve, Isolation of bacteria and 16S rDNAs from Lake Vostok accretion ice, Environ. Microbiol. 3 (2001) 570–577.
[8] J.A. Raymond, B.C. Christner, S.C. Schuster, A bacterial ice-binding protein from the Vostok ice core, Extremophiles 12 (2008) 713–717.
[9] A.M. Achberger, T.I. Brox, M. Skidmore, B. Christner, Expression and partial characterization of an ice-binding protein from a bacterium isolated at a depth of 3519 m in the Vostok ice core, Antarctica, Front. Microbiol. 2 (2011) 255.
[10] H.M. Mader, Observations of the water vein system in polycrystalline ice, J. Glaciol. 38 (1992) 333–347.
[11] W.M. Ketcham, P.V. Hobbs, An experimental determination of the surface energies of ice, Philos. Mag. 162 (1969) 1161–1173.
[12] P.B. Price, A habitat for psychrophiles in deep Antarctic ice, Proc. Natl. Acad. Sci. U.S.A. 97 (2000) 1247–1251.
[13] R.L. Sutton, A. Lips, G. Piccirillo, A. Sztehlo, Kinetics of ice recrystallization in aqueous fructose solutions, J. Food Sci. 61 (1996) 741–745.
[14] A.J. Bray, Theory of phase-ordering kinetics, Adv. Phys. 51 (2002) 481–587.
[15] H. Kirsebom, D. Topgaard, I.Y. Galaev, B. Mattiasson, Modulating the porosity of cryogels by influencing the nonfrozen liquid phase through the addition of inert solutes, Langmuir 26 (2010) 16129–16133.
[16] H. Kirsebom, G. Rata, D. Topgaard, B. Mattiasson, I.Y. Galaev, *In situ* H-1 NMR studies of free radical cryopolymerization, Polymer 49 (2008) 3855–3858.
[17] Y.Q. Song, H. Cho, T. Hopper, A.E. Pomerantz, P.Z. Sun, Magnetic resonance in porous media: recent progress, J. Chem. Phys. (2008) 128.
[18] J.R. Brown, T.I. Brox, S.J. Vogt, J.D. Seymour, et al., Magnetic resonance diffusion and relaxation characterization of water in the unfrozen vein network in polycrystalline ice and its response to microbial metabolic products, J. Magn. Reson. 225 (2012) 17–24.
[19] M.W. Hunter, R. Dykstra, M.H. Lim, T.G. Haskell, P.T. Callaghan, Using earth's field NMR to study brine content in Antarctic sea ice: comparison with salinity and temperature estimates, Appl. Magn. Reson. 36 (2009) 1–8.
[20] H. Raich, P. Blumler, Design and construction of a dipolar Halbach array with a homogeneous field from identical bar magnets: NMR Mandhalas, Concepts Magn. Reson. Part B 23B (2004) 16–25.
[21] R. Knight, E. Grunewald, T. Irons, K. Dlubac, et al., Field experiment provides ground truth for surface nuclear magnetic resonance measurement, Geophys. Res. Lett. (2012) 39.
[22] J. Takagi, B.M. Petre, T. Walz, T.A. Springer, Global conformational rearrangements in integrin extracellular domains in outside-in and inside-out signaling, Cell 110 (2002) 599–611.
[23] S.N. Montross, M. Skidmore, B. Christner, D. Samyn, Debris-rich basal ice as a microbial habitat, Taylor Glacier, Antarctica, Geomicrobiol. J. 31 (2014) 76–81.
[24] R. Valiullin, I. Furo, The morphology of coexisting liquid and frozen phases in porous materials as revealed by exchange of nuclear spin magnetization followed by H-1 nuclear magnetic resonance, J. Chem. Phys. 117 (2002) 2307–2316.
[25] P.T. Callaghan, Principles of Nuclear Magnetic Resonance Microscopy, Oxford University Press, New York 1991, 2014.
[26] K.R. Brownstein, C.E. Tarr, Importance of classical diffusion in NMR studies of water in biological cells, Phys. Rev. A 19 (1979) 2446–2453.
[27] P.P. Mitra, P.N. Sen, L.M. Schwartz, Short time behavior of the diffusion coefficient as a geometrical probe of porous media, Phys. Rev. B 47 (1993) 8565–8574.
[28] P.N. Sen, Time-dependent diffusion coefficient as a probe of geometry, Concept. Magn. Reson A 23A (2004) 1–21.
[29] R.W. Mair, M.D. Hurlimann, P.N. Sen, L.M. Schwartz, et al., Tortuosity measurement and the effects of finite pulse widths on xenon gas diffusion NMR studies of porous media, Magn. Reson. Im. 19 (2001) 345–351.
[30] L.E. Reichl, A Modern Course in Statistical Physics, University of Texas Press, Austin 1980, 2014.
[31] R.W. Mair, G.P. Wong, D. Hoffmann, M.D. Hurlimann, et al., Probing porous media with gas diffusion NMR, Phys. Rev. Lett. 83 (1999) 3324–3327.
[32] C.P. Garnham, R.L. Campbell, P.L. Davies, Anchored clathrate waters bind antifreeze proteins to ice, Proc. Natl. Acad. Sci. U.S.A. 108 (2011) 7363–7367.
[33] C. Richardson, Phase relationships in sea ice as a function of temperature, J. Glaciol. 17 (1976) 507–519.
[34] G.M. Marion, M.V. Mironenko, M.w. Roberts, FREZCHEM: A geochemical model for cold aqueous solutions, Comput. Geosci. 36 (2010) 10–15.
[35] M.D. Hurlimann, K.G. Helmer, L.L. Latour, C.H. Sotak, Restricted diffusion in sedimentary rocks- determination of surface-area-to-volume-ratio and surface relaxivity, J. Magn. Reson. A 111 (1994) 169–178.
[36] K.M. Cuffey, W.S.B. Paterson, The Physics of Glaciers, Elsevier, 2010.
[37] D. Dahl-Jensen, N. Gundestrup, Constitutive properties of ice at Dye 3, Greenland. The physical basis of ice sheet modeling, IAHS 170 (1987) 31–43.
[38] Herron S.L, Langway C.C Jr., Brugger K.A, C.C. Langway Jr., Ultrasonic velocities and crystalline anisotropy in the ice core from Dye 3, Greenland, in: Oeschger H, Dansgaard W (Eds.), Greenland Ice Core: Geophysics, Geochemistry, and the Environment, AGU, Washington D.C, 1985.
[39] K.M. Cuffey, H. Conway, A. Gades, B. Hallet, et al., Deformation properties of subfreezing glacier ice: role of crystal size, chemical impurities, and rock particles inferred from in situ measurements, J. Geophys. Res. 105 (2000) 27895–27915.